NASA/TM—2014-216615

Burst Testing of Triaxial Braided Composite Tubes

J.A. Salem
Glenn Research Center, Cleveland, Ohio

J.L. Bail
Ohio Aerospace Institute, Brook Park, Ohio

N.G. Wilmoth
Vantage Partners, LLC, Brook Park, Ohio

L.J. Ghosn, L.W. Kohlman, G.D. Roberts, and R.E. Martin
Glenn Research Center, Cleveland, Ohio

January 2014

NASA STI Program . . . in Profile

Since its founding, NASA has been dedicated to the advancement of aeronautics and space science. The NASA Scientific and Technical Information (STI) program plays a key part in helping NASA maintain this important role.

The NASA STI Program operates under the auspices of the Agency Chief Information Officer. It collects, organizes, provides for archiving, and disseminates NASA's STI. The NASA STI program provides access to the NASA Aeronautics and Space Database and its public interface, the NASA Technical Reports Server, thus providing one of the largest collections of aeronautical and space science STI in the world. Results are published in both non-NASA channels and by NASA in the NASA STI Report Series, which includes the following report types:

- TECHNICAL PUBLICATION. Reports of completed research or a major significant phase of research that present the results of NASA programs and include extensive data or theoretical analysis. Includes compilations of significant scientific and technical data and information deemed to be of continuing reference value. NASA counterpart of peer-reviewed formal professional papers but has less stringent limitations on manuscript length and extent of graphic presentations.

- TECHNICAL MEMORANDUM. Scientific and technical findings that are preliminary or of specialized interest, e.g., quick release reports, working papers, and bibliographies that contain minimal annotation. Does not contain extensive analysis.

- CONTRACTOR REPORT. Scientific and technical findings by NASA-sponsored contractors and grantees.

- CONFERENCE PUBLICATION. Collected papers from scientific and technical conferences, symposia, seminars, or other meetings sponsored or cosponsored by NASA.

- SPECIAL PUBLICATION. Scientific, technical, or historical information from NASA programs, projects, and missions, often concerned with subjects having substantial public interest.

- TECHNICAL TRANSLATION. English-language translations of foreign scientific and technical material pertinent to NASA's mission.

Specialized services also include creating custom thesauri, building customized databases, organizing and publishing research results.

For more information about the NASA STI program, see the following:

- Access the NASA STI program home page at *http://www.sti.nasa.gov*

- E-mail your question to *help@sti.nasa.gov*

- Fax your question to the NASA STI Information Desk at 443–757–5803

- Phone the NASA STI Information Desk at 443–757–5802

- Write to:
  STI Information Desk
  NASA Center for AeroSpace Information
  7115 Standard Drive
  Hanover, MD 21076–1320

NASA/TM—2014-216615

Burst Testing of Triaxial Braided Composite Tubes

J.A. Salem
Glenn Research Center, Cleveland, Ohio

J.L. Bail
Ohio Aerospace Institute, Brook Park, Ohio

N.G. Wilmoth
Vantage Partners, LLC, Brook Park, Ohio

L.J. Ghosn, L.W. Kohlman, G.D. Roberts, and R.E. Martin
Glenn Research Center, Cleveland, Ohio

National Aeronautics and
Space Administration

Glenn Research Center
Cleveland, Ohio 44135

January 2014

Acknowledgments

Thanks to Chris Burke for running tube tests.

Level of Review: This material has been technically reviewed by technical management.

Available from

NASA Center for Aerospace Information
7115 Standard Drive
Hanover, MD 21076–1320

National Technical Information Service
5301 Shawnee Road
Alexandria, VA 22312

Available electronically at http://www.sti.nasa.gov

Burst Testing of Triaxial Braided Composite Tubes

J.A. Salem
National Aeronautics and Space Administration
Glenn Research Center
Cleveland, Ohio 44135

J.L. Bail
Ohio Aerospace Institute
Brook Park, Ohio 44142

N.G. Wilmoth
Vantage Partners, LLC
Brook Park, Ohio 44142

L.J. Ghosn, L.W. Kohlman, G.D. Roberts, and R.E. Martin
National Aeronautics and Space Administration
Glenn Research Center
Cleveland, Ohio 44135

Abstract

Applications using triaxial braided composites are limited by the materials transverse strength which is determined by the delamination capacity of unconstrained, free-edge tows. However, structural applications such as cylindrical tubes can be designed to minimize free edge effects and thus the strength with and without edge stresses is relevant to the design process. The transverse strength of triaxial braided composites without edge effects was determined by internally pressurizing tubes. In the absence of edge effects, the axial and transverse strength were comparable. In addition, notched specimens, which minimize the effect of unconstrained tow ends, were tested in a variety of geometries. Although the commonly tested notch geometries exhibited similar axial and transverse net section failure strength, significant dependence on notch configuration was observed. In the absence of unconstrained tows, failure ensues as a result of bias tow rotation, splitting, and fracture at cross-over regions.

Introduction

Triaxial braided composite employing large-tow-size yarns offer a good combination of cost and performance for many aerospace applications. One factor limiting the performance of such composites is the effect of free tow-ends: sections with terminated tow-ends subjected to tensile loads exhibit low strength relative to sections with constrained tow ends. The failure mechanisms have been studied by Littell et al. (Ref. 1), and imply tow splitting and delamination at edges subjected to load.

Because tow-end stresses and related edge effects can be minimized in structures such as tubes and spheres, it is of interest to measure the transverse strength both with and without free-end effects. Standard straight-sided uniaxial test specimens (e.g., ASTM D3039) exhibit these edge effects and do not represent the potential of the material under certain design condition because the load resolved on the unconstrained edge tows causes damage to propagate along the tow. On the other hand, it will be shown in this work that failure progression in pressurized tubes, as observed by interruption of pressure tests, occurs by delamination at bias tow edges via a scissoring action. Delamination is followed by longitudinal splitting and then transverse breakage of split tows where the bias tows cross the axial tows. The low strength of transverse tensile specimens is thus a structural effect.

The strength without edge effects can be measured by employing partially pressurized tubes because the overhung regions are subjected to substantially lower hoop stresses than the highly loaded central region. The length of overhang can be used to interrogate the sensitivity to edge stress and the transition from internal failure to edge failure. Another advantage of a tubular geometry is its geometric similarity to applications such as aircraft engine cases, which are critical to efficiency and safety, and are locally loaded during rotating component failure.

Besides tubes, uniaxial specimens can be designed to either restrain free-end-tows or shield restrained tows such that strength reduction is mitigated. Examples of such specimens are the bowtie and edge-notched sheet specimens that restrain the tows passing through the ligament. Transverse tests with these specimens indicate similar net section ultimate strengths to D3039 axial values for T700S/E-862 carbon-epoxy composite (Refs. 2 and 3). FEA of notched tensile specimens subjected to fixed grip ends implies that the free edges, where unconstrained tows exist, are shielded from significant load via the notch. However, the notch does create a stress concentration and audible damage occurs at relatively low load levels. Thus the effect of notch geometry on resultant tensile strength was examined in this work as a function of notch angle and depth. Although tubes and notched uniaxial specimens can be compared, complications occur because of the different defects caused by the more complex manufacturing process required for tubes as compared to that used for flat plates. These effects were partially mitigated by visual inspection of the tubes.

The purpose of this work was to apply tube testing methods generally employed for testing monolithic ceramics, ceramic matrix composites and graphite to polymer composite materials and thereby measure the strength in the absence of terminated tows. For comparison, notched specimens were also tested.

Tubes can be pressurized by bladders or with fluids such as oil (Refs. 4 to 7), however, fluids are messy and hard to contain under large displacements and the high pressures and displacements required for polymer composites make the use of bladders more difficult. Using a polymer insert as a pressurization medium has been used previously with relatively stiff materials such as ceramics (Ref. 8), however, application to relatively compliant strong materials such as polymer composites present the additional complication of large displacements, high pressures, and extrusion of the insert.

Mosley has done substantial investigation into tube testing of ceramics and put forth detailed recommendations (Ref. 8) for infinite length tubes. As composite materials are expensive to manufacture, a short tube that results in sufficiently low edge stress relative to the maximum stress is desirable. Reuter and Guess (Ref. 7) derived an elegant criterion for the minimum overhang to eliminate edge effects in short tubes and demonstrated strength improvements in the absence of edge effects. Besides being short, a uniform wall stress with low second and third principal stresses is needed as the transverse uniaxial tensile strength is of interest. Further, simple strength of materials solutions should be reasonably descriptive.

Results for tubes and multiple notch geometries are presented with the goal of understanding failure behavior and the limits of simple notched coupon tests.

Test Method Verification

Finite Element Analysis

Because of the large displacements associated with high strength, low stiffness materials such as polymer composites (S_f = 120 ksi, E = 7×10^6 psi), containment of the polymer plug was of concern. Thus tube pressurization in combination with and without edge constraint was considered. Finite element analysis (FEA) results are shown in Figures 1 and 2. Edge constraint proved difficult due to the sharp transition between constrained and unconstrained regions. Thus simple pressurization over a short region (~1/3rd) via a low durometer insert was pursued. For this case, a peak hoop stress occurs about the centerline and is accompanied by a small axial stress. For practical purposes, all stresses at the free edges are zero, as shown in Figure 2.

The size of the pressure zone is critical to the stress distribution through the wall and the ratio of axial to hoop stress. As shown in Figure 3 for 6 in. isotropic tubes, a zone of 1.875 in. produces uniform stress through the wall and separates the axial peaks from the hoop peaks making it a quasi-uniaxial test. Longer pressurized zones approach the strength-of-materials solution, with the peak stress on the inner wall. However, the peak axial and hoop stresses coincide. Thus a 1.88 to 2 in. zone was used in experiments.

For notched tensile specimens subjected to fixed grip ends, strain concentrations are exhibited, as shown in Figure 4. However, the concentration in a composite is strongly associated with the tows terminated at the notch root. All gripped tows exhibit a very uniform strain and the terminated tows at specimen edges are practically strain free. Thus the load capacity of the tows crossing the ligament are employed.

Although the stress concentration is significant, such effects in composites are less governed by Saint-Venant's principle and tend to be transmitted over larger areas. Thus the concentration might be mitigated via fiber architecture and end restraints.

Experimental Stress Analysis

High strength aluminum, which has a similar elastic modulus to the composite, was used for experimental verification of tube testing. Pressurization was achieved by compressing a polymer plug between platens. Strain was monitored by using a photogrammetry system and associated software (Trilion Quality Systems). The elastic constants of the tube material were determined by compressing the tube while monitoring the surface displacements via the camera system.

Pressurization of the tube resulted in excellent agreement with theory for an infinite tube, as shown in Figure 5. The bending induced axial stress at the mid-plane is ~12 percent of the maximum hoop stress. However, by the time the hoop stress decays significantly (~5 percent); the axial stress has increased to ~25 percent of the hoop. Observations of failure locations in composite tubes, discussed in the following sections, indicated mid-plane failure, implying that the state is sufficiently uniaxial for engineering purposes.

Test Materials and Experimental Procedures

The composites were made with high strength, standard modulus TORAYCA T700S fiber (Toray Carbon Fibers America, Inc.) and EPIKOTE Resin 862/EPIKURE with Curing Agent W (Resolution Performance Products) or 5208 one part resin. Fiber and resin properties reported by the fiber manufacturers are shown in Table 1. The 2D triaxial braid preforms were made by A&P Technology (A&P Technology), and composite panels and tubes were fabricated by resin transfer molding (RTM) at North Coast Composites (North Coast Composites).

A representative picture of the 0/+60/–60 triaxial braid architecture unit cell is shown in Figure 6. The ±60° bias fibers are visible on the surface, and portions of the 0° axial fibers that lie below the ±60° bias fibers can be seen in open spaces. The 0° axial fibers were 24k flattened tows while the ±60° bias fibers were 12k flattened tows. Although larger fiber bundles were used in the axial direction, the fiber bundle spacing in the axial and bias directions were adjusted to give the same fiber volume in the axial and bias directions. This fiber architecture is quasi-isotropic in-plane, so the in-plane stiffness is expected to be the same in all directions when the region of measurement includes several unit cells.

Composite plates were fabricated by placing 12 layers of the 0/+60/–60 braid preform into the RTM mold with the 0° fibers aligned in the same direction. Although the axial (0°) fibers in the various layers were parallel, the lateral position in the six layers was not controlled, but typically exhibited shifting often referred to as nesting. The braided composite tubes were manufactured by over-braiding six layers of triaxial braid on a mandrel, followed by RTM. The fiber volume fraction, braid angle, tow selection, and cure conditions were chosen to match, as closely as possible, the parameters of the flat panel material. The lateral position of the axial tows in the tubes were clocked slightly, creating nesting and improving consolidation. Also, the preforming methods and molding procedures were adjusted as successive tubes

were fabricated in order to reduce defects and optimize the process. As a result, some of the tubes had known defects (mainly local distortion of fiber tows) prior to testing.

Resin was injected into the closed mold and cured according to processing conditions recommended by the resin manufacturer. The E862 was cured for 2 1/2 hr at 177 °C (350 °F) and the 5208 was cured for 2 hr at 177 °C (350 °F). Cured panel dimensions (after trimming) were 2 ft wide by 2 ft long by 0.25 in. thick. Cured tube dimensions were 24 in. long with 4.17 in. outer diameter (OD) and 3.91 in. inner diameter (ID). Some of the tubes were observed to have defects (mainly distortion of fiber tows) prior to testing.

Uniaxial tensile specimens were cut from the panels by using an abrasive water jet followed by fine grinding. Straight-sided specimens were prepared and tested in accordance with ASTM International D3039. The transverse and axial notch configurations are summarized by Figure 7. Relative notch depths of 2a/W = 0.5 and 0.8 were used with notch angles between 0° to 120° in order to understand notch sensitivity. A relative depth of 0.8 leaves sufficient material for one unit cell. Uniaxial tests were performed at a stroke rate of 0.050 in./min which typically gave a strain rate of 1 to 1.5×10^{-4}/s. Typically, five or more specimens were tested per condition. For tubes, a nominal pressure rate 68 psig/s was applied to produce a hoop strain rate of 1.5×10^{-4}/s.

Photogrammetry (digital image correlation) was used to monitor both global and local strain fields by choosing a gage length larger than the local architecture or within a region of interest.

Stresses in a Finite Tube

The nominal tensile stress in the central region of an infinite isotopic tube can be estimated from

$$\sigma_t = \frac{R_i^2 p_i}{R_o^2 - R_i^2}\left(1 + \frac{R_o^2}{r^2}\right) \tag{1}$$

$$\sigma_r = \frac{R_i^2 p_i}{R_o^2 - R_i^2}\left(1 - \frac{R_o^2}{r^2}\right) \tag{2}$$

$$\sigma_{\max} = \frac{R_i^2 p_i}{R_o^2 - R_i^2}\left(1 + \frac{R_o^2}{R_i^2}\right) \tag{3}$$

where p_i is the applied internal pressure, R_i is inner radius, R_o is the outer radius, and r is the radial position of interest. Based on Equations (1) to (3), the maximum principal stress is tangential (hoop) and occurs on the ID. This is not the exact case for a partially pressurized tube as the free, overhung ends constrain expansion of the central region and thereby cause axial bending stresses. Also, small frictional effects may occur. Despite these effects, the full elastic solutions considering the constraint (Ref. 8) were within 4 percent of strength-of-materials (SOM) values (Eq. (3)).

Results

Uniaxial Strength

Axial and transverse, macro-level stress-strain curves are shown in Figure 8 for T700S/E862 and / 5208. For transverse loading, nonlinear extension occurs at ~0.5 percent strain and ~25 percent of the ultimate axial strength. A linear regression fit range of 0.5 percent, which was larger than that used previously (0.2 percent, (Ref. 1)), provided more consistency in Poisson's ratio and met reciprocity requirements ($\nu_{12}/E_{11} = \nu_{21}/E_{22}$) with $E_{11} = 6.95\times10^3$ ksi, $\nu_{12} = 0.34$, $E_{22} = 6.03\times10^3$ ksi, and $\nu_{21} = 0.30$, as shown in Table 2.

T700S/5208 exhibited less nonlinear extension prior to failure and lower fracture strength. The effects of notch angle and depth are shown in Figure 9, and imply that net section strength decreases with increasing notch angle for transverse and axial orientations. For transverse orientation, large angles cut bias tows thereby resulting in less length of bias tows through which load can be transmitted, and less shielding, via surrounding material, of tows that do carry load through the ligament. Interestingly, shallow notches exhibit lower strength than deep notches again implying that additional material to the side of a tow shields the loaded tow: unsupported tows running along a free edge (e.g., 60 notch) are weaker.

Axial specimens are most sensitive to notches, with deep notches exhibiting the greatest net section strength, implying significant edge effects even in well machined, unnotched sections. Notching improves axial strength by shedding load to bias tows crossing the ligament and mitigating machining damage to the load bearing tows. Further, all load bearing tows are supported by surrounding material, thereby maximizing load redistribution. The notched axial values converge to somewhat below the smooth section value, implying a small stress concentration effect once edge effects are mitigated.

The notched specimen is simple to fabricate and forces fiber tensile failure for transverse specimens by constraining free-end tows subjected to load. Although notched specimens have a non-uniform gage region and resultant stress concentrations, notched coupons produced higher strength values compared to the straight-sided coupon. This is due to the structural nature of the composite and resultant notch insensitivity.

Noteworthy for notched specimens was early, audible popping during loading and nonlinearity at about 60 ksi, implying that the notch does influence damage initiation. However, propagation and ultimate failures were limited by tow restraint: all bias fibers passing through the ligament are restrained within the grip and carry load. For axial specimens, failure begins with separation of the ears from the ligament by transverse splitting of bias tows along the interface between notched and un-notched sections, as shown in Figure 10(a). As the notch angle is increased, the maximum axial strains shift from the interface region to the bias tows intersecting the edges, weakening the section. For transverse specimens, failure begins with high strains in bias tow intersecting the notch root. The strains gradually migrate inward along the ligament centerline until distinct jumps in bias tow strain levels (~2 percent) occur due to delamination. Large, horizontal bands of high strain can be seen in some axial tows, as shown in Figure 10(c).

For large notch angle (120°), bias tows along the notch edges also exhibit large strains, weakening the specimens, as shown in Figure 10(d). For deep notches, highly strained bias tows can be seen to extent to the grips.

Noteworthy for unnotched transverse specimens is the strain banding shown in Figure 11. These local strain concentrations and the applied stress were used to estimate local, effective elastic Young's modulus and Poisson's ratio. These *in situ* measurements gave $E = 7.74\times10^3$ ksi and $\nu = 0.41$ for the low strain regions between 0° tows and $E = 5.11\times10^3$ ksi with $\nu = 0.25$ in the high strain regions corresponding to tows. This is ~±10 percent from the macro-level modulus values. Non-linear strains are exhibited in high strain regions at about two-thirds the applied stress required to create non-linearity in the low strain regions, and the equality of transverse strains implies good compatibility between regions, Figure 11(c). For the axial tests, banding is less apparent and the macro values are representative.

The low strength in transverse loading has been described (Refs. 1 and 3) as the result of tow splitting, outward delamination, and pull-out of a terminated tow. The delamination and splitting occurs because the resolved tow loads are only supported by surrounding epoxy. Besides notching, which gives acreage for load shedding, continuity of the tows, as occurs in tubes, can be used to mitigate this structural affect.

Tubular Strength

Tube burst strength is compared to straight sided, bowtie, and notched section tensile strength in Table 3 for T700S/E862. Partial pressurization of tubes and notching of tensile specimens results in comparable transverse strength estimates (118 vs. 119 ksi). Some difficulty was encountered in failing several tubes. The loads were sufficient to partially extrude the plug between the platen and tube wall,

implying that the plug was too soft. These tests were not included in reported averages, but the loads implied potential strength greater than 140 ksi.

The axially woven tubes failed from the center where maximum hoop stress occurred, as shown in Figure 12, with an explosive report. The transverse wrapped tubes failed by delamination at the braid end rather than by fiber failure. This resulted in low and more variable strengths. Stress-strain curves for tubular and transverse uniaxial specimens are compared in Figure 13. The tubes exhibit linear behavior to near maximum stress and give little indication of damage until stresses are comparable to the uniaxial strength in the axial direction. Ultimate strains are ~1.8 percent which is near that of the yarn (~2.1 percent). Most interesting is the tendency of the tubes to stiffen just after the failure stress exhibited by straight-sided uniaxial transverse tests (dotted horizontal lines in Fig. 13). This presumably occurs from locking of the braid and engagement of the bias fibers.

Significant strength variation between specimens taken from different tubes (90 to 125 ksi) was exhibited and most failures occurred within one tow repeat of a mold line. The variation was traced predominantly to variation the quality of the braid architecture and section thickness near the mold-lines. Two sources of low strength were identified: fiber distortion or curved fibers at the mold lines and damaged or cut fibers. Figure 14(a) shows the stress—strain curve for a specimen with cut fibers. The tube exhibited low compliance and strain relaxation at the central gage region as the specimen delaminated between the cut and uncut lamina shown in Figure 14(b). Failure occurred at only 90 ksi. Figure 14(c) shows a specimen with distorted fibers on one side of a mold-line. Although the initial compliance is nearly that of well molded specimens, large strains were exhibited at the mold-line as the fibers straightened. The large mold line strains resulted in strain relaxation between the mold lines where the optical strain gage was placed. Failure occurred just below the mold line where the fibers were distorted, Figure 14(c). The strain enhancement associated with distorted fibers can be seen in detail for another tube in Figure 15. The values in Tables 3 and 4 represent measurements from tubes of good visual quality. The strongest tube (~135 ksi) was comparable to the axial strength measured in the presence of a deep notch.

When axial load is applied parallel to a curved tow, it rotates and aligns to the applied load direction causing local deformation and weakness. Although properties might be improved by minimizing braid distortions and gaps between tows, regions exhibiting the most apparent distortions did not always exhibit failure. Failure may be controlled by distortion occurring through multiple layers.

Due to the coarse architecture and associated stiffness variations, the axial overbraided tubes exhibit substantial strain variation in the hoop direction for any axial position, as shown in Figure 16, with high strains corresponding to axial tows, and overall agreement with Figure 3. As pressure increases, specific axial tows exhibit large surface strains (~5 percent) that persist until failure. At relatively high pressures, regions initially exhibiting low hoop strain in axial tows develop significant hoop strain (~4 percent) in the pattern of the bias tows. Thus the choice of location and size of the strain gage can affect interpretation of results. In order to estimate the stress and strain distributions and variations during the failure process, strain measurements were averaged for multiple “hot” and “cold” regions.

As shown in Figure 17, substantial nonlinear extension occurs prior to failure in some regions, and the strains at axial tows are more than double those between tows, Figure 17(a). Once the axial tows exhibit non-linear strain, which occurs simultaneously in hoop and longitudinal directions at ~2 percent hoop strain, the bias tows shed hoop strain while increasing longitudinal strain, Figure 17(b). Thus the axial tows shed load to the bias tows as failure ensues and the system globally stiffens. The bias tows in a tube can take extra load because they are contiguous. Figures 8 and 17 imply that the ultimate strength and the onset of damage are significantly improved relative to transverse uniaxial loading, with the onset of nonlinear behavior occurring at ~75 percent of ultimate for T700S/E862. The global stiffening might be used as an indicator of localized damage.

Tube data for T700S/5208 is summarized in Table 4. Figure 9 implies that deep notches (2a/W = 0.8 with θ = 0° to 60°) give the most comparable results to tubes for the current architecture. Clearly, notched specimens show systematic dependence on notch depth and angle for both transverse and axial orientations. It is noteworthy that both the strongest notched specimens and the tubes that presented testing difficulty due to plug extrusion exhibited nominal stresses of 140 ksi, implying that tube strength can be improved. More study of notched geometry effects is needed with various epoxies to give specific recommendations.

Failure Mode

Observations of partially failed tubes indicated that as axial tows subject to transverse loads relax, the tube stiffens by engagement of the bias tows, Figure 18. Failure of tubes ensues as the bias tows rotate parallel to the hoop stress and delaminate along tow edges, Figure 18(a). Delamination and further loading leads to impingement of the fibers at cross-over regions and a scissoring action that splits the tows, Figure 18(b). Eventually, tow breakage occurs where bias tows cross over axial tows, Figure 18(c), resulting in expulsion of a single axial tow as shown in Figure 12(a).

Thus the increased strength exhibited by notched specimens is a structural effect of more load being transmitted along bias tows, elimination of edge damage, and sheltering of tows carrying load. Even a well prepared axial specimen with free edges will be weaker because of the unrestrained tows and low delamination strength. Making the tows contiguous and retaining free material to the side of bias tows, as in a tube or deeply notched specimen, improves structural integrity by employing the load carrying capability of all tows.

Conclusions

Triaxially braided composites exhibited substantial anisotropy and heterogeneity on the scale of tows, despite the repeating pattern. This created large local strain variation and high delamination stresses at free-edge tows. The use of overhung tubes eliminated the influence of unrestrained free-end tows, allowing estimation of the areal strength as opposed to the edge strength. The hoop strength of axially overbraided tubes was comparable to uniaxial measurements of the axial strength and to the net-section transverse strength when free-end tows were restrained and sheltered via notching. Although tube pressurization results in a mildly biaxial stress state, the hoop and axial stress maximums can be separated to some extent by pressurizing a short region. This also results in a uniform hoop stress through the tube wall. Distortions in the fiber architecture and section thickness, which usually occurred near mold lines, occasionally caused strain concentrations and low tube strength. Axially wrapped tubes, in which the ply end was not restrained, exhibited low strength due to ply delamination. Failure of hoop loaded axial braided tubes ensued by relaxation of axial tows, rotation of bias tows that caused delamination, tow impingement and system stiffening, longitudinal tow splitting, and eventual failure where the bias tows cross axial tows.

Notched uniaxial transverse specimens exhibited similar strength to tubes and axial specimens, however, some dependence on notch angle and depth exists, and nonlinear strain occurs earlier. In the case of notched axial specimens, the dependence is the result of load shedding to bias tows. In the case of transverse specimens, the dependence is the result of shielding of the bias tows from a free edge: the restrained tows crossing the ligament act as structural elements or “tie rods” that connect the load grips. Unconstrained tows only transmit load thru the surrounding epoxy. Depending on the notch design and orientation, the areal strength can be under or overestimated. For transverse orientation, underestimates tend to occur. For deeper notches, which have more surrounding material, higher strength is exhibited. Effective use of all tows by restraint is a key aspect for strength optimization.

References

1. J.D. Littell, W.K. Binienda, G.D. Roberts, and R.K. Goldberg, "Characterization of Damage in Triaxial Braid Composites Under Tensile Loading," NASA/TM—2009-215645.
2. C.L. Bowman, G.D. Roberts, M.S. Braley, M. Xie, and M.J. Booker, "Mechanical Properties of Triaxial Braided Carbon/Epoxy Composites," in 35th International SAMPE Technical Conference—vol. 35, Sept. 29-Oct. 2, 2003, Dayton OH (SAMPE Covina, CA 2003).
3. L.W. Kohlman, J.L. Bail, G.D. Roberts, J.A. Salem, R.E. Martin, W.K. Binienda, "A notched coupon approach for tensile testing of braided composites," Composites Part A: Applied Science and Manufacturing, Volume 43, Issue 10, October 2012, Pages 1680–168.
4. S. Schwentes and W. Elber, "Slow Crack Growth in Spinel in Water," NASA Technical Memorandum 85644, May 1983.
5. J.A. Salem and J.Z. Gyekenyesi, "Burst Pressure Testing of Ceramic Rings," NASA TM—2007-214695, 2007.
6. M.J. Verrilli, J.A. DiCarlo, A. Calomino, H.M. Yun, and T.R. Barnett, "Hoop Tensile Properties of Ceramic Matrix Composite Cylinders," Journal of Testing and Evaluation, vol. 33, no. Sept. 2005.
7. R.C. Reuter and T.R. Guess, "Analysis, Testing, and Design of Filament Wound, Carbon-Carbon Burst Tubes," Composite Materials: Testing and Design, ASTM STP 546, pp. 67–83, 1974.
8. K. Mosley "The Stressing for Test Purposes of Materials in Tubular Form Using Elastomeric Inserts – Experimental and Theoretical Development," Proc. Inst. Mech. Eng., vol. 196, pp. 124–139, 1982.

TABLE 1.—FIBER AND RESIN PROPERTIES

Fiber	Tensile strength, ksi (MPa)	Young's modulus, msi (GPa)	Failure strain, percent	Density, lb/in.^{3} (g/cm^3)
T700S	711 (4900)	33.4 (230)	2.1	0.065 (1.80)
E862	8.8 (61)	0.39 (2.7)	------	0.043 (1.270)
5208	7.3 (50)	0.56 (3.8)	------	0.046 (1.20)

TABLE 2.—ELASTIC CONSTANTS FOR TRIAXIAL BRAID COMPOSITE AT 0.5 PERCENT STRAIN

Material	E_{11}, (msi)	E_{22}, (msi)	ν_{12}	ν_{21}
E862/T700	6.95±0.23	6.03±0.12	0.34	0.30
5208/T700	6.69±0.24	6.23±0.25	0.29	0.29

TABLE 3.—TENSILE STRENGTH OF T700S/E862 MEASURED WITH VARIOUS CONFIGURATIONS (ksi)

Orientation	Tube (Central pressurization)	D3039 tensile	60° Notched tensile	0° Notched tensile
Axial	90.3±7.8 (3)	118±4 (5)	117±1 (2)	112±13 (2)
Transverse	119±6 (3)	67.3±5.2 (5)	125±4 (4)	118±17 (2)

TABLE 4.—TENSILE STRENGTH OF T700S/5208 MEASURED WITH VARIOUS CONFIGURATIONS (ksi)

Orientation	Tube (Central pressurization)	D3039 tensile	60° Notched tensile	0° Notched tensile
Axial	----------	106±8 (6)	109±9 (5)	118±4 (5)
Transverse	113±4 (4)	44±2 (6)	----------	100±12 (5)

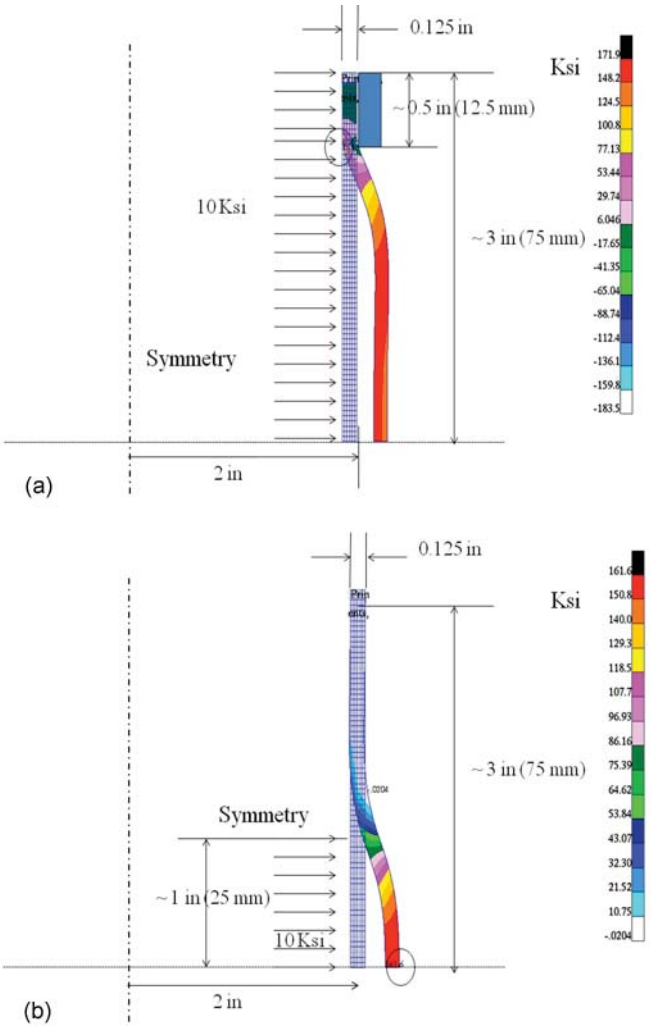

Figure 1.—Maximum principal stresses for (a) constrained edge and (b) free edge conditions.

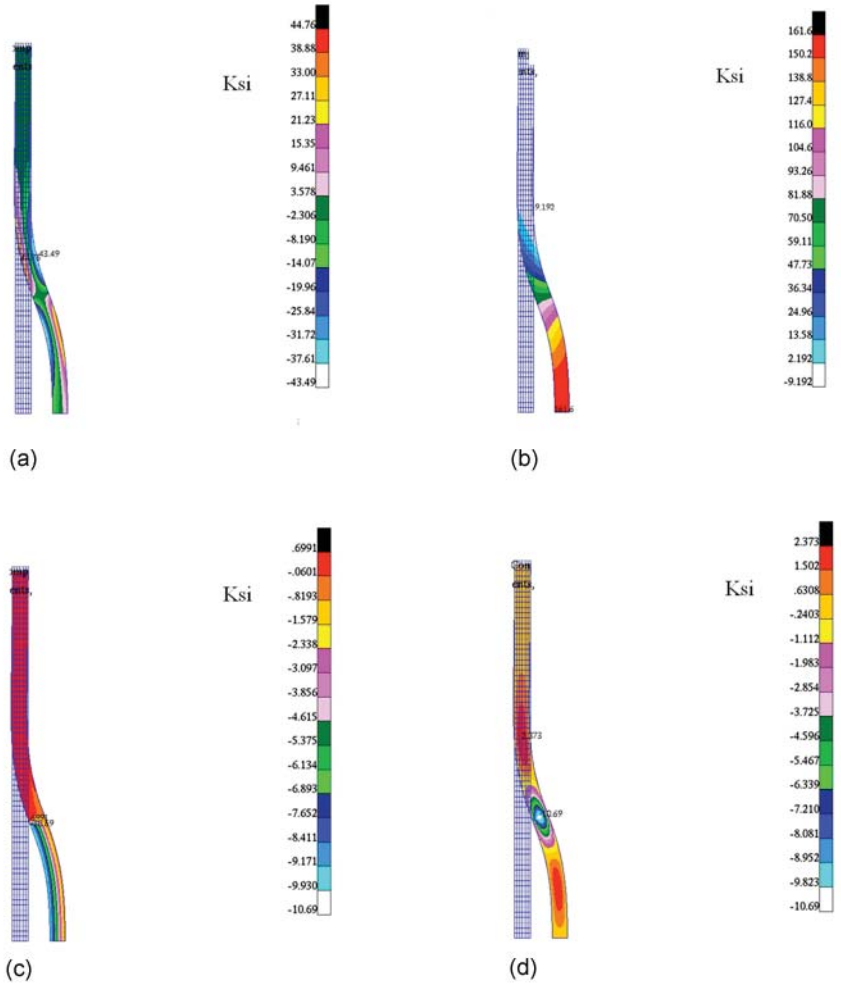

Figure 2.—Stress distributions in a partially pressurized tube: (a) axial, (b) hoop, (c) radial, and (d) shear.

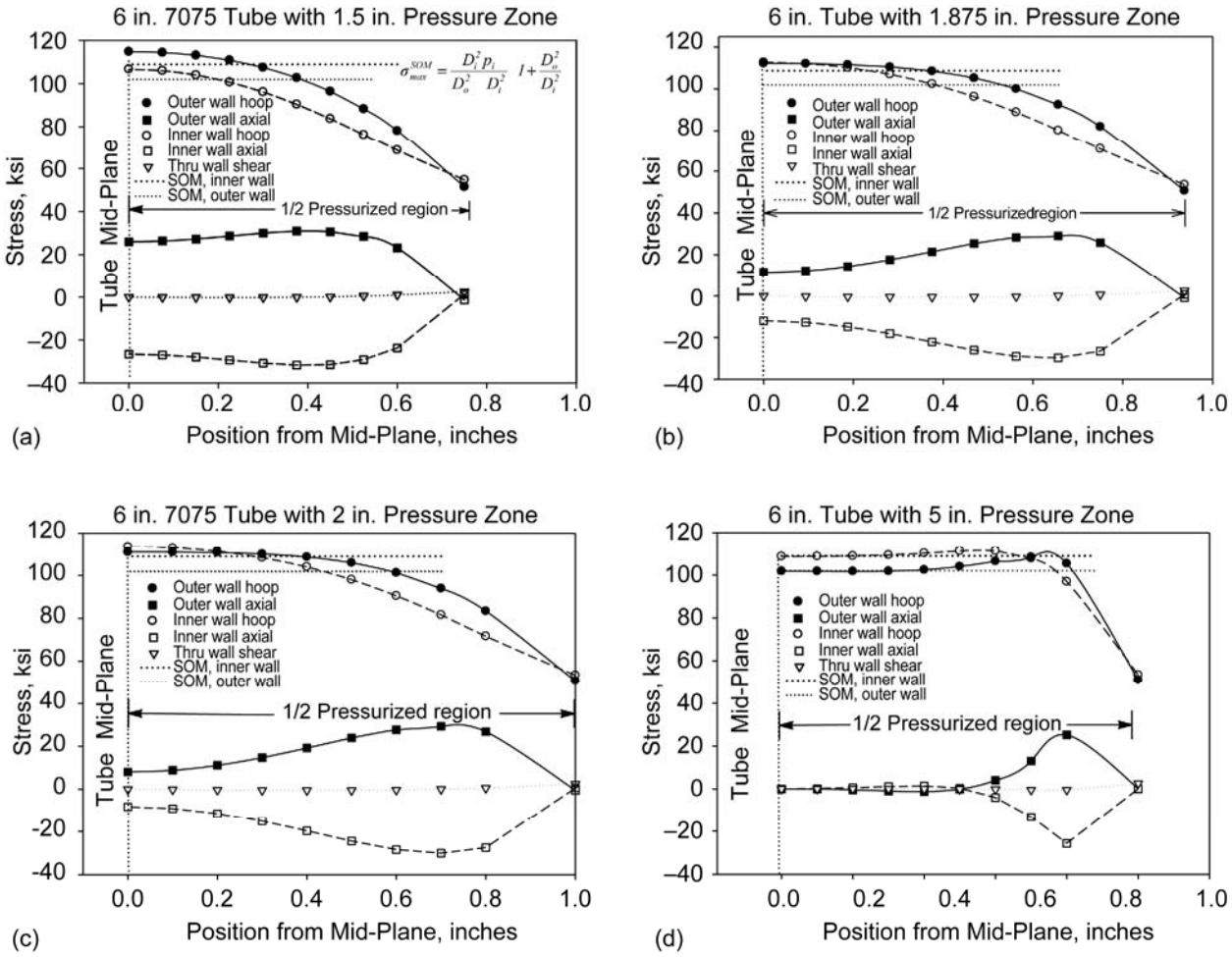

Figure 3.—Stress distribution in a 6 in. partially pressurized isotropic tube: (a) 1.5 in. zone, (b) 1.875 in. zone, (c) 2 in. zone, and (d) 5 in. zone.

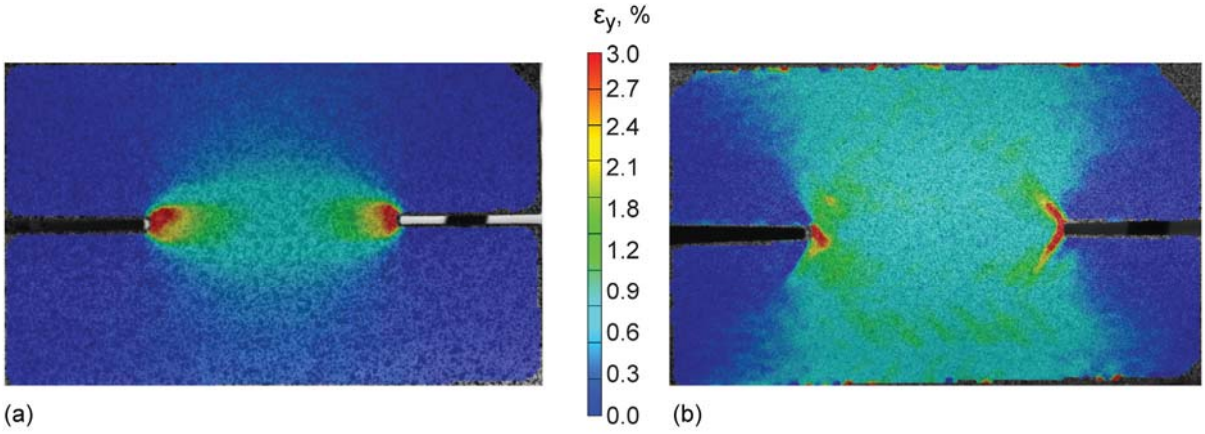

Figure 4.—Strain distribution in an (a) aluminum and (b) triaxial braided composite notch tensile specimen subjected to fixed-end loading.

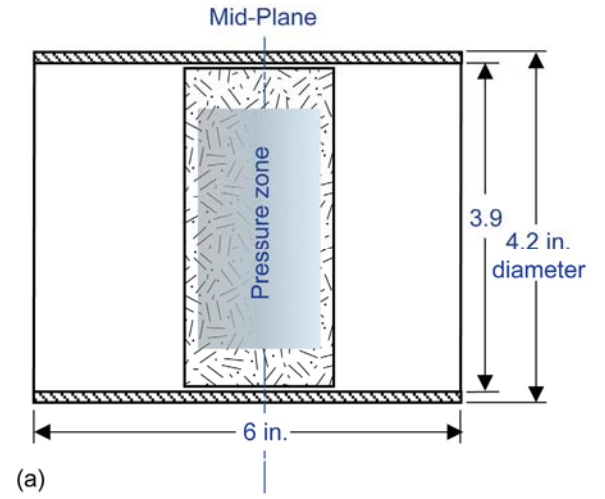

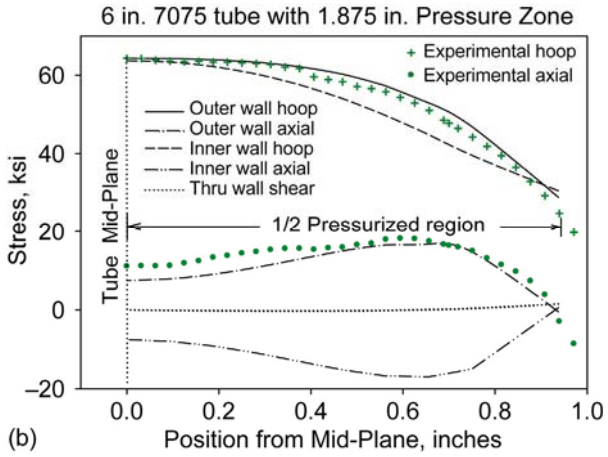

Figure 5.—(a) Tube schematic and (b) experimentally measured and theoretical stresses for a partially pressurized infinite aluminum tube (half-symmetry).

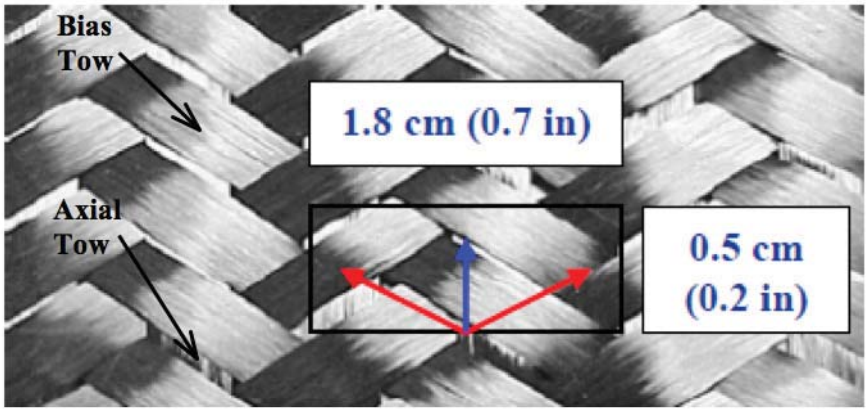

Figure 6.—Two-dimensional triaxial braid carbon fiber preform with highlighted unit cell. The blue arrow indicates the axial fiber direction, and the red arrows indicate bias fiber directions.

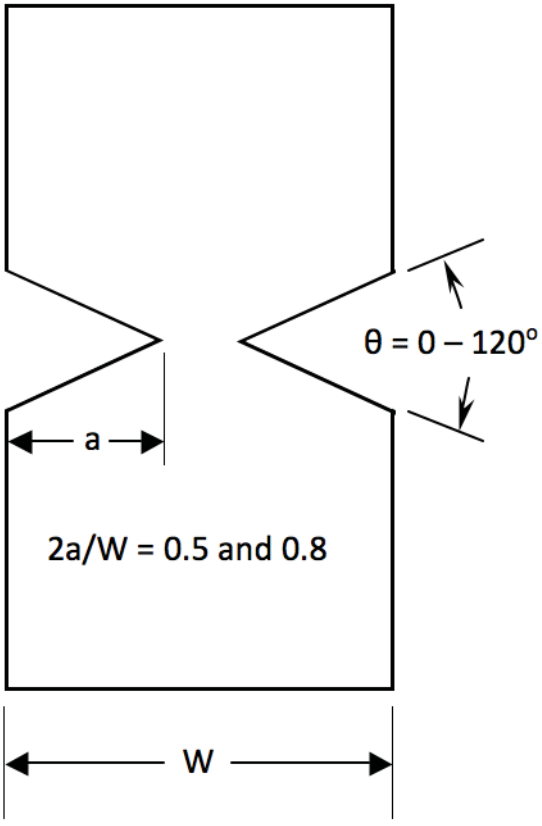

Figure 7.—Notched tensile configuration.

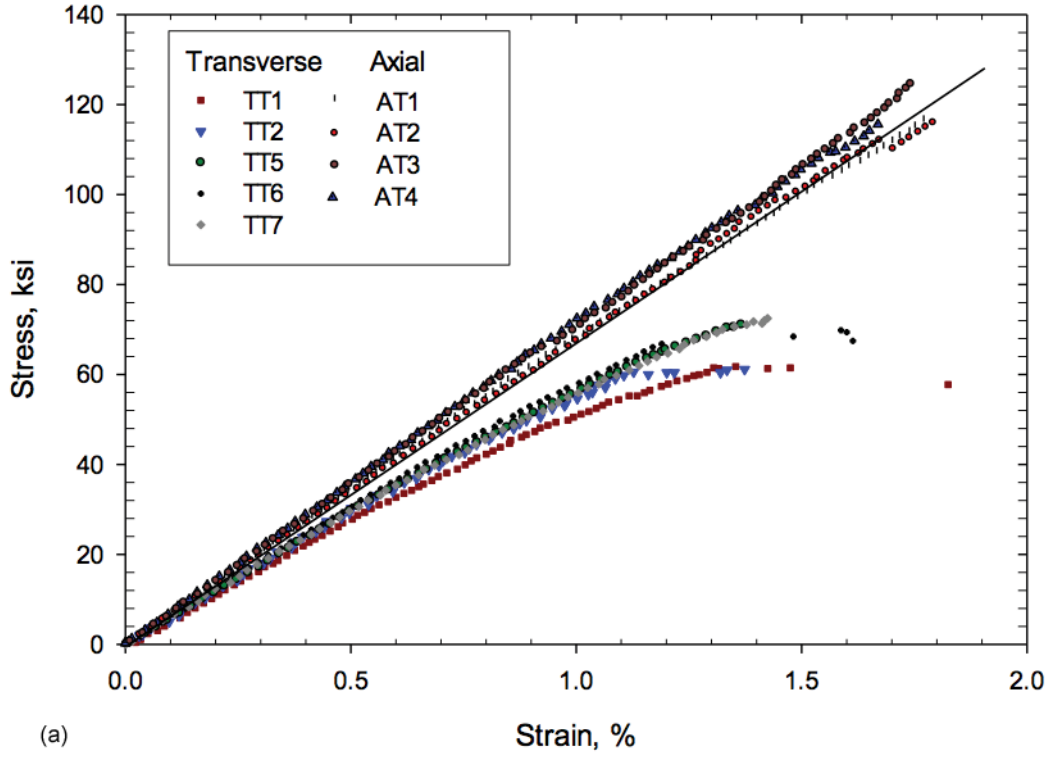

(a)

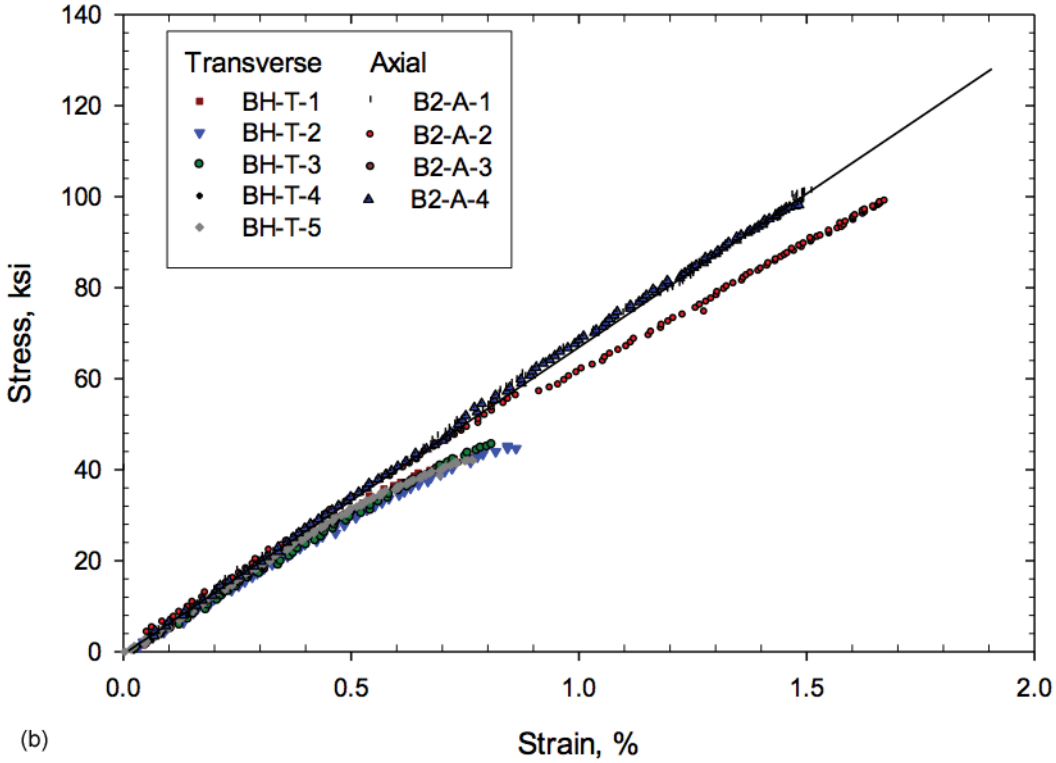

(b)

Figure 8.—ASTM D3039 axial and transverse global stress-strain curves for (a) T700S/E862 and (b) T700S/5208.

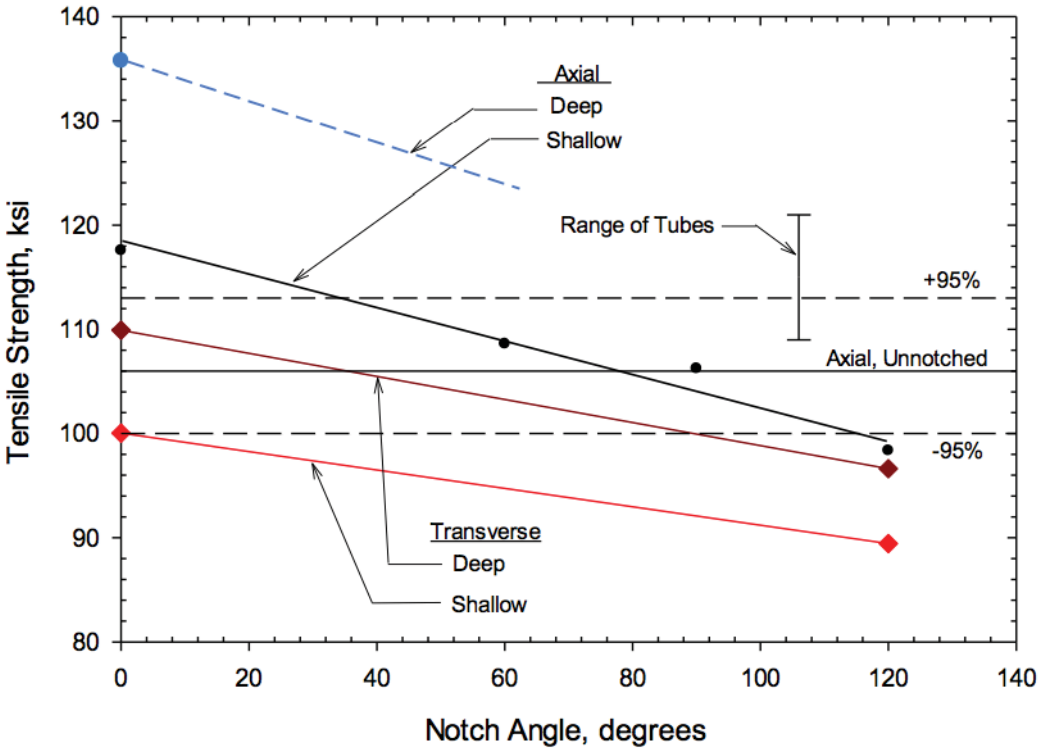

Figure 9.—Uniaxial net section strength as function of notch angle and depth for T700S/5208.

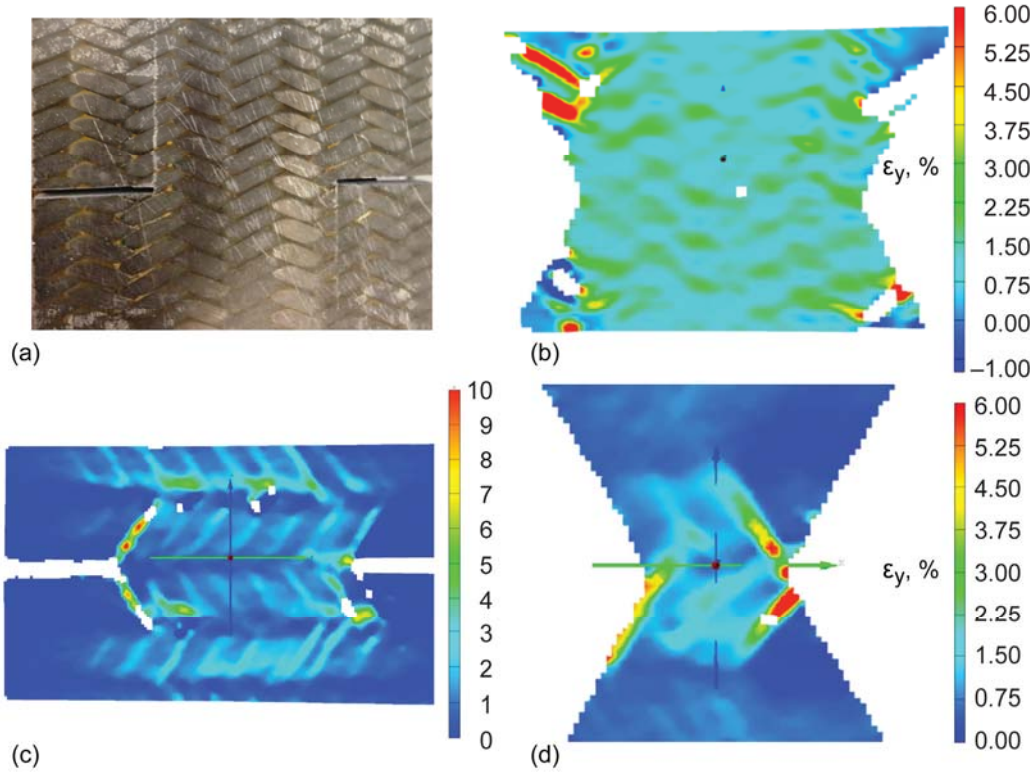

Figure 10.—Examples of notched axial tensile tests: (a) splitting between notched and unnotched regions; (b) axial strain distribution about a 120° notch. Examples of notched transverse tests: (c) strain concentrations at bias tows and strain banding at tow intersections; (d) strain concentration along a 120° free edge.

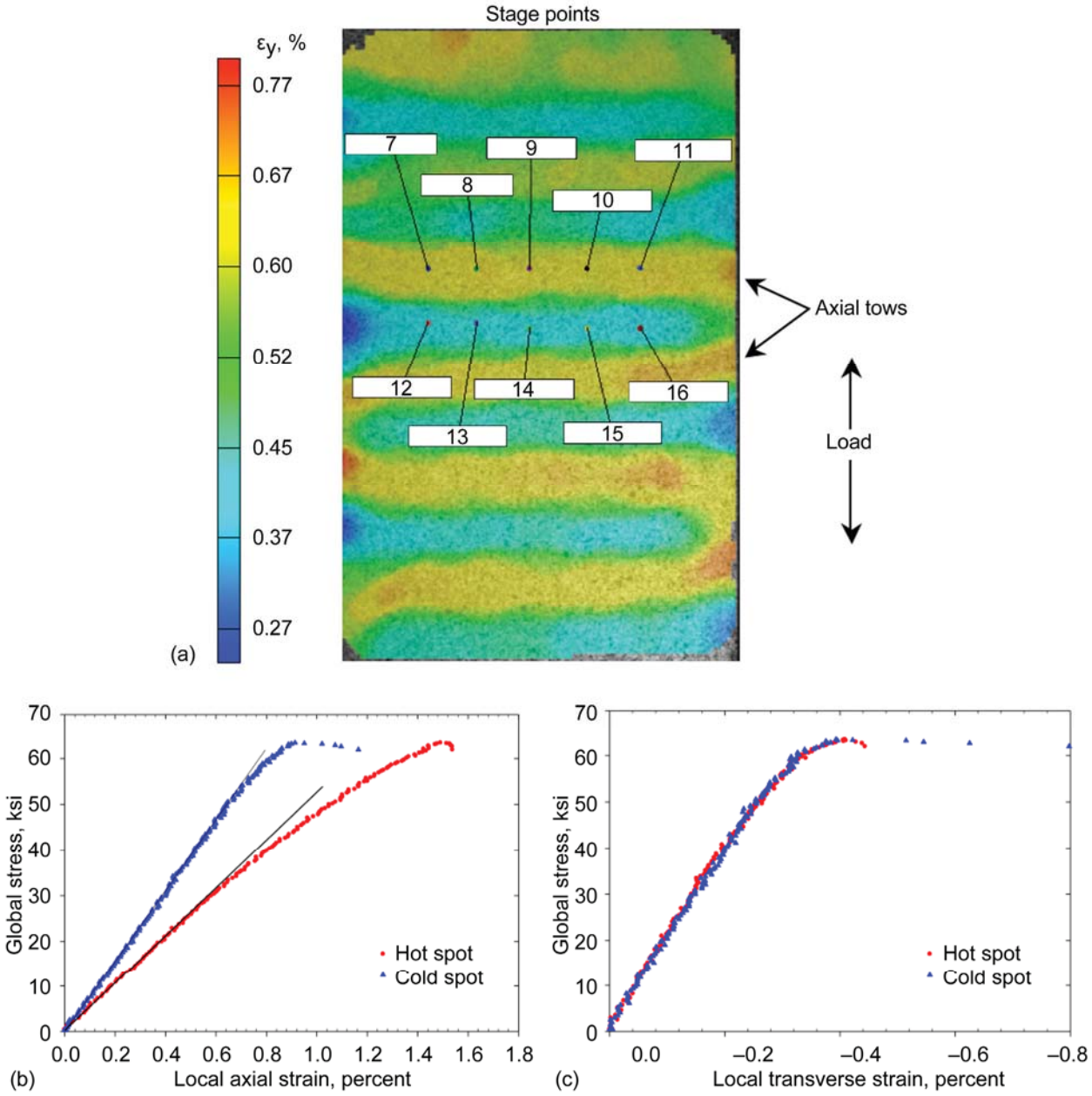

Figure 11.—Strain banding at 32 ksi (a) and correspond axial (b) and transverse (c) stress-strain curves for the high and low strain regions of a T700/5208 transverse tensile test.

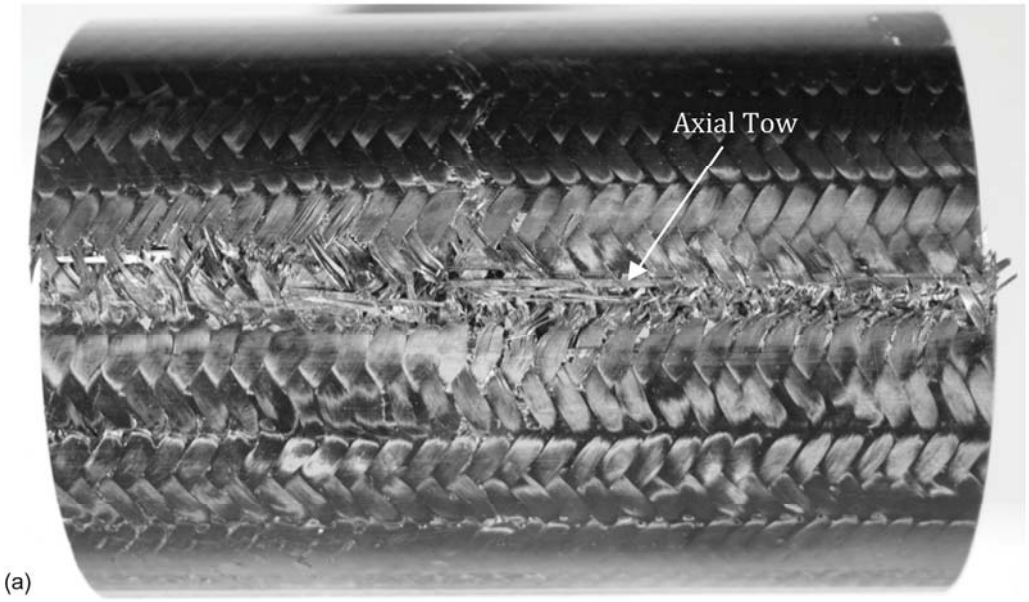

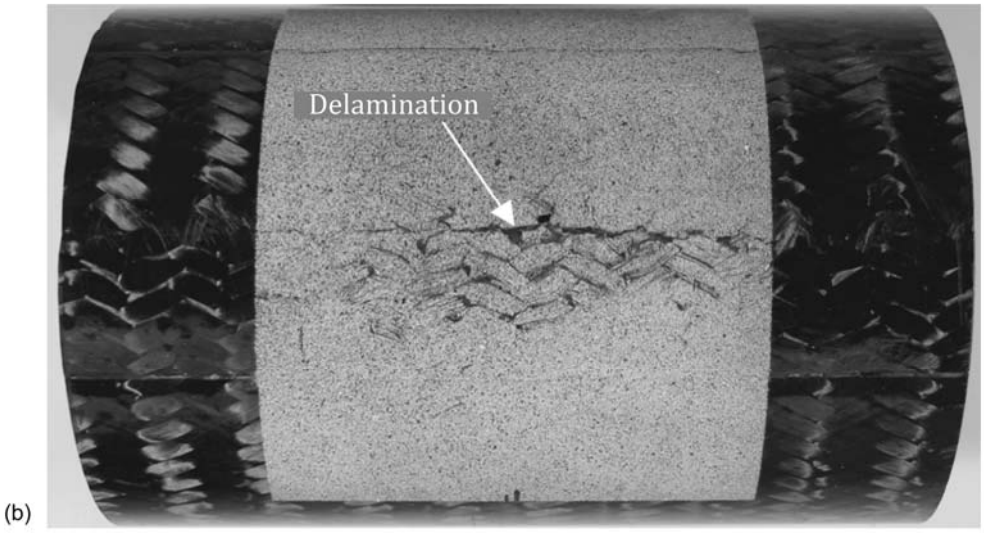

Figure 12.—Burst tubes with (a) axial tows in axial direction, and (b) axial tows in hoop direction.

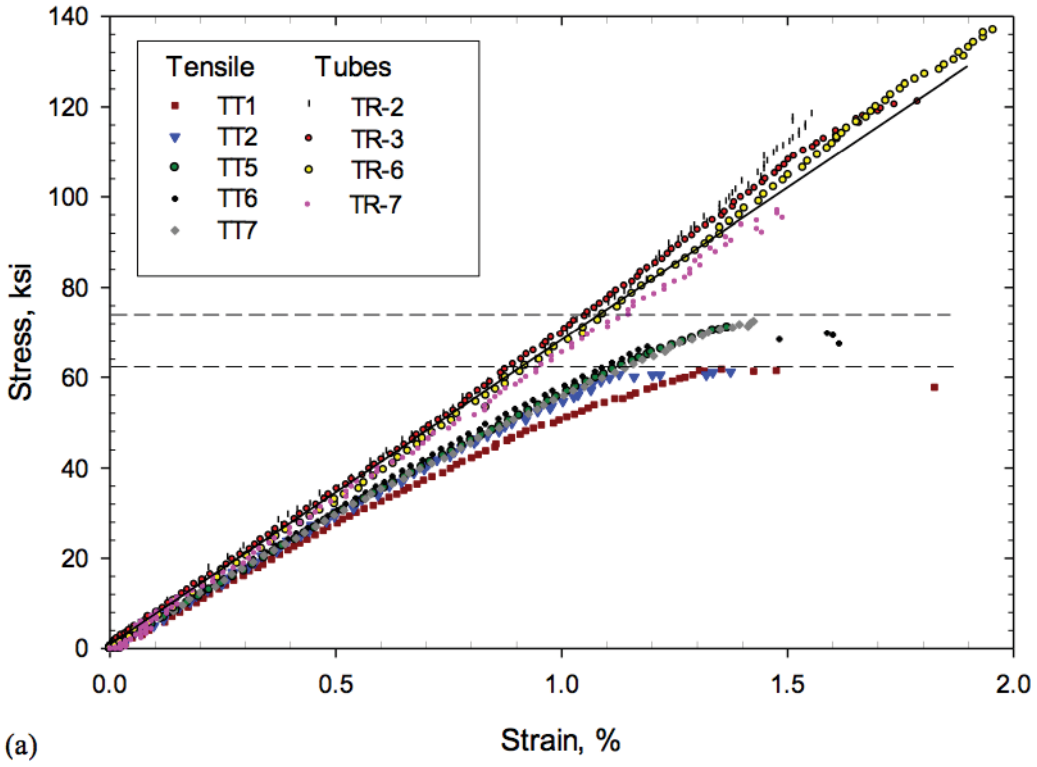

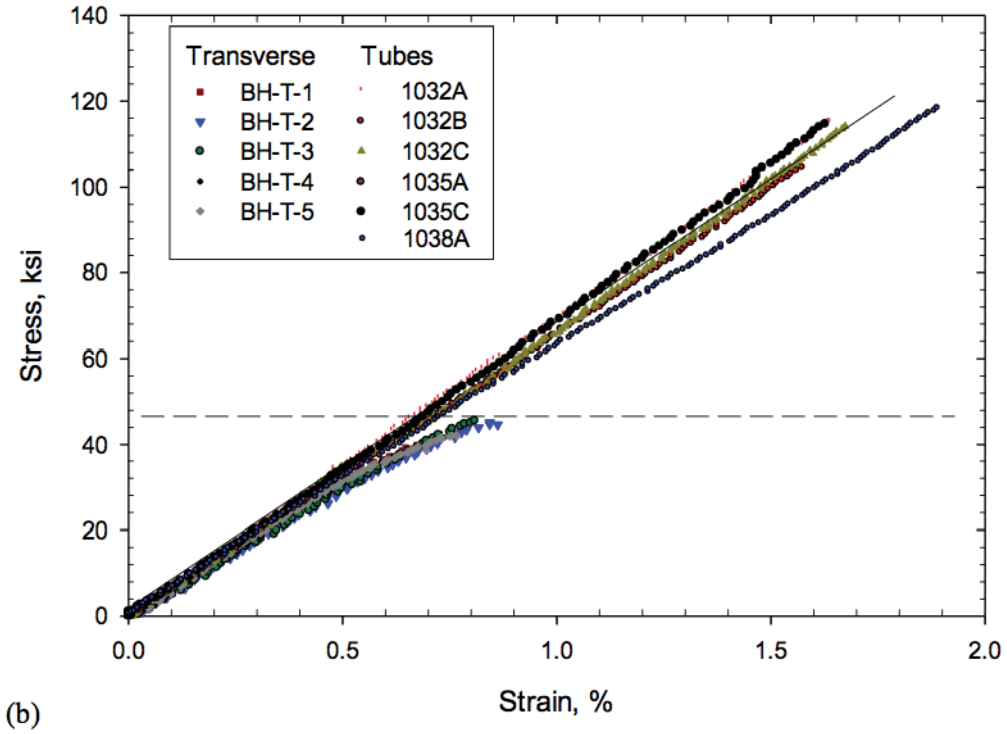

Figure 13.—Strength-of-materials stress for (a) T700S/E862 and (b) T700S/5208 as a function of strain for pressurized axially-woven tubes and ASTM D3039 transverse tensile specimens.

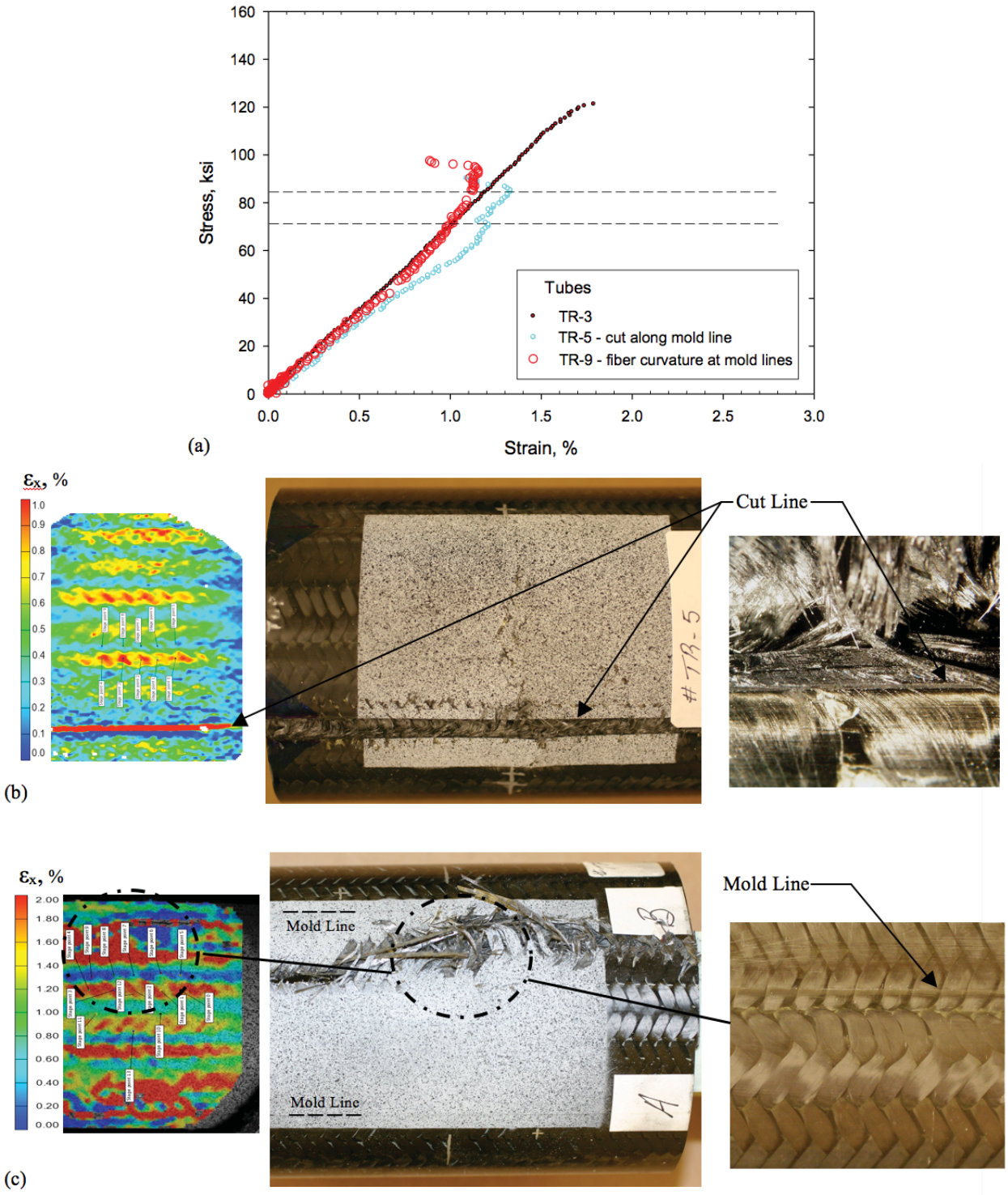

Figure 14.—(a) Stress-strain curves for T700S/E862 tubes with (b) damaged (TR-5 at 34 ksi) and (c) distorted fibers at mold lines (TR-9 at 89 ksi).

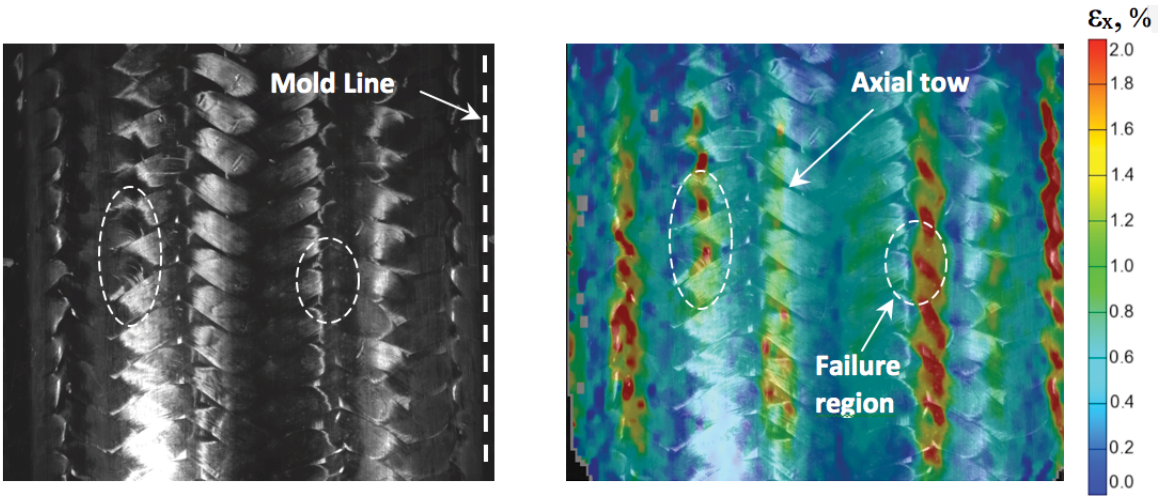

Figure 15.—Hoop strain enhancement at distorted fibers and axial tows in an axially woven T700s/E862 tube (TR-7) at 45 percent of failure (44 ksi).

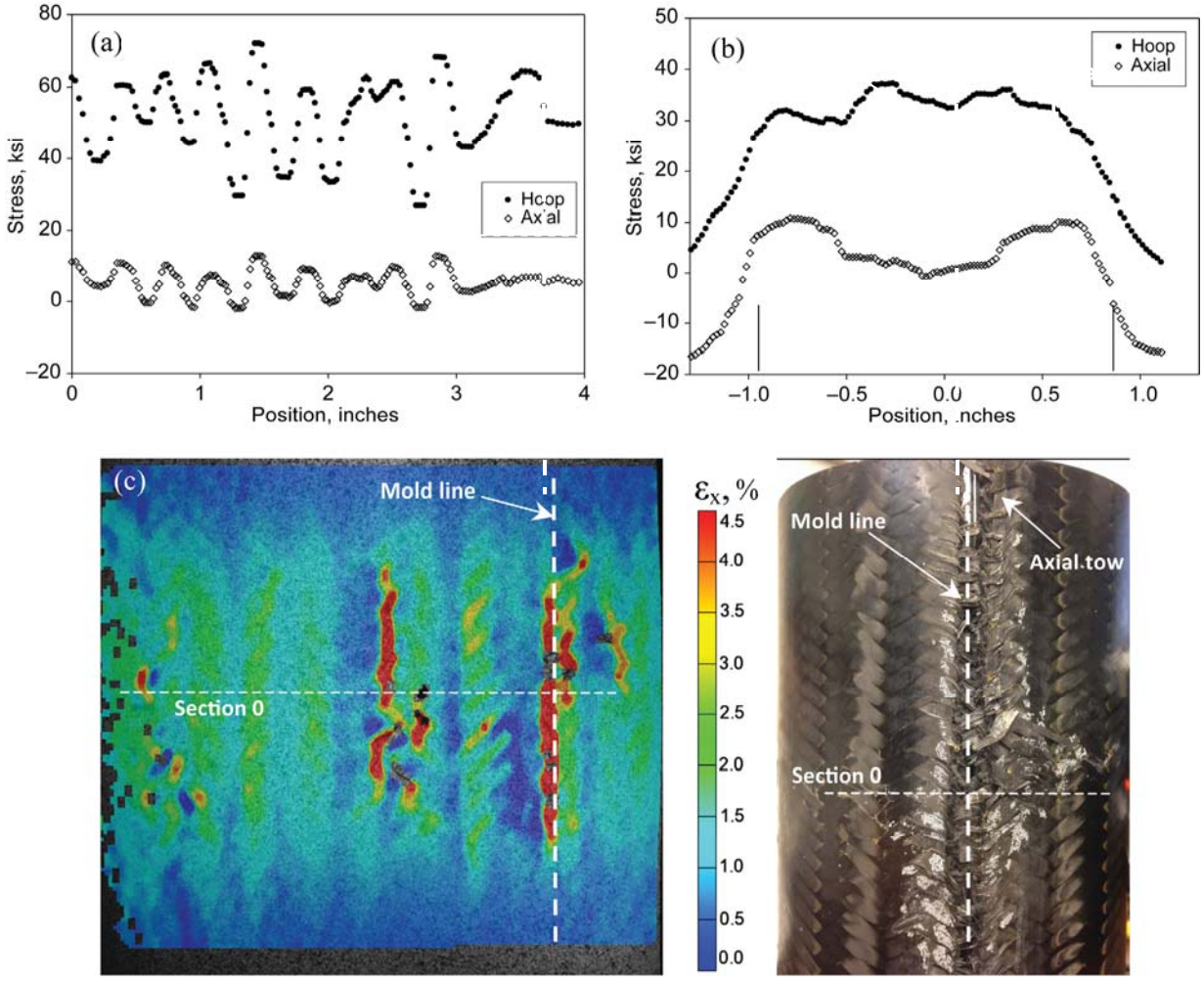

Figure 16.—Strength-of-materials stress variation in a T700S/E862 pressurized tube (TR-3) along (a) tube circumference, (b) tube longitudinal axis at a SOM stress of 52 ksi, (c) strain variation at 104 ksi, and (d) burst tube.

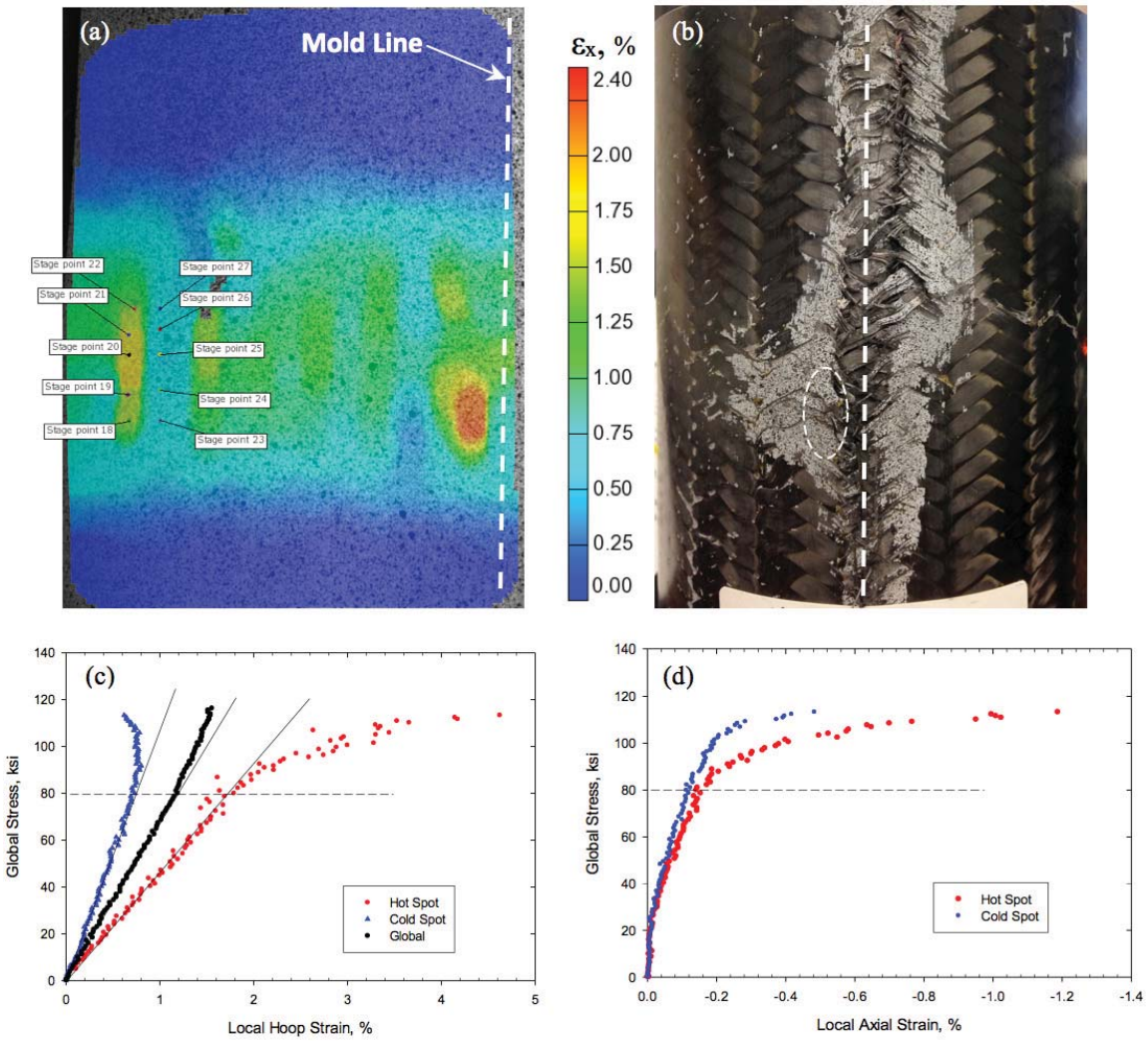

Figure 17.—Stress as a function of strain for high and low strain regions of a T700S/E862 pressurized tube (TR-2): (a) local strain gages and high strain region near mold line at 72 ksi, (b) failed tube, (c) hoop (ε_x) strain, and (d) axial (ε_y) strain).

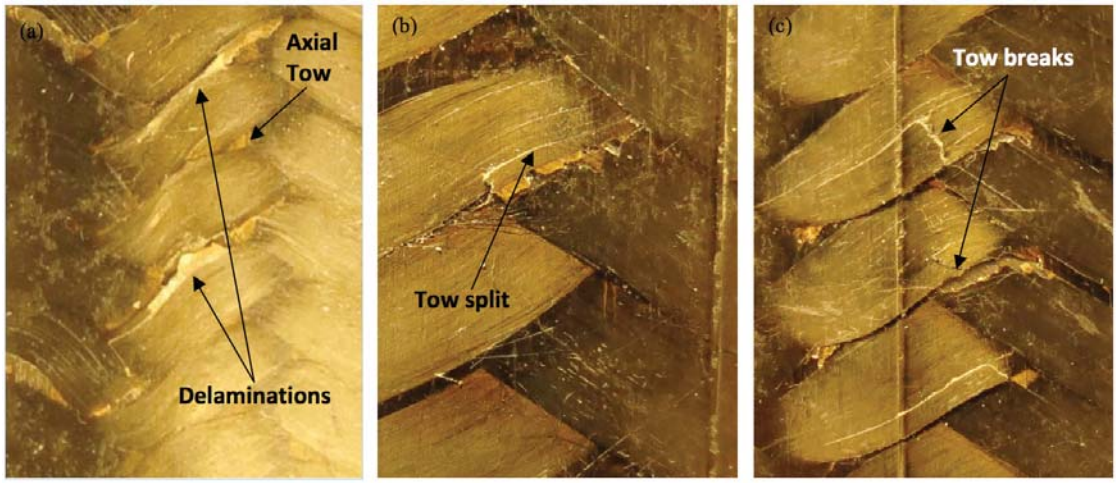

Figure 18.—Examples of tow delamination, splitting, and breakage occurring just before failure in a pressurized T700S/5208 tube (1035B).